Astron. Astrophys. 330, 1–9 (1998)

ASTRONOMY
AND
ASTROPHYSICS

Arc statistics with realistic cluster potentials

IV. Clusters in different cosmologies

Matthias Bartelmann[1], **Andreas Huss**[1], **Jörg M. Colberg**[1], **Adrian Jenkins**[2], **and Frazer R. Pearce**[2]

[1] Max-Planck-Institut für Astrophysik, P.O. Box 1523, D-85740 Garching, Germany
[2] Physics Department, University of Durham, Durham DH1 3LE, UK

Received 21 July 1997 / Accepted 17 October 1997

Abstract. We use numerical simulations of galaxy clusters in different cosmologies to study their ability to form large arcs. The cosmological models are: Standard CDM (SCDM; $\Omega_0 = 1$, $\Omega_\Lambda = 0$); τCDM with reduced small-scale power (parameters as SCDM, but with a smaller shape parameter of the power spectrum); open CDM (OCDM; $\Omega_0 = 0.3$, $\Omega_\Lambda = 0$); and spatially flat, low-density CDM (ΛCDM; $\Omega_0 = 0.3$, $\Omega_\Lambda = 0.7$). All models are normalised to the local number density of rich clusters. Simulating gravitational lensing by these clusters, we compute optical depths for the formation of large arcs. For large arcs with length-to-width ratio ≥ 10, the optical depth is largest for OCDM. Relative to OCDM, the optical depth is lower by about an order of magnitude for ΛCDM, and by about two orders of magnitude for S/τCDM. These differences originate from the different epochs of cluster formation across the cosmological models, and from the non-linearity of the strong lensing effect. We conclude that only the OCDM model can reproduce the observed arc abundance well, while the other models fail to do so by orders of magnitude.

Key words: galaxies: clusters: general – cosmology: dark matter – cosmology: gravitational lensing – cosmology: large-scale structure of Universe

1. Introduction

Galaxy clusters form differently in different cosmological models. Their formation history and their internal structure are influenced by the cosmological parameters. In dense model universes, $\Omega_0 \sim 1$, clusters form at significantly lower redshifts than in low-density model universes (e.g. Richstone, Loeb, & Turner 1992; Bartelmann, Ehlers, & Schneider 1993; Lacey & Cole 1993, 1994). The cosmological constant has a fairly moderate influence on the formation timescale. Delayed formation is reflected in the abundance of cluster substructure. Moreover, central cluster densities are higher in clusters that form earlier.

It is currently unclear whether the different degrees of cluster substructure expected in cosmological models with different mean densities lead to observational consequences that can significantly distinguish between high- and low-density universes. While earlier studies found cluster X-ray morphologies and density profiles to differ significantly between different cosmologies (Evrard et al. 1993; Crone, Evrard, & Richstone 1994; Mohr et al. 1995; Crone, Evrard, & Richstone 1996), more recent work concluded that X-ray morphologies of clusters at the present epoch are fairly similar in different cosmological models, rendering significant distinctions difficult (Jing et al. 1995). The issue of constraining cluster shapes using their X-ray emission was also addressed in detail by Buote & Tsai (1995a,b). The weak gravitational lensing effect allows a measurement of the morphology of the projected mass (Wilson, Cole, & Frenk 1996; Schneider & Bartelmann 1997) and constrains cluster density profiles (Crone et al. 1997), but it remains to be shown with realistic numerical cluster models whether this method provides a more sensitive tool to quantify cluster morphologies than that provided by X-ray emission.

An alternative tool is offered by the strong gravitational lens effect. In order to be strong lenses (i.e. in order to produce appreciable numbers of large arcs from background sources), clusters have to satisfy several criteria. First, they need to be compact, that is, their central surface mass densities need to surmount the critical surface mass density for lensing. The latter depends on redshift. For background sources at redshifts $z_\mathrm{s} \sim 1$, clusters at redshifts $0.2 \lesssim z_\mathrm{c} \lesssim 0.4$ are the most efficient lenses. If arcs are to be produced in abundance, a sufficiently large number of concentrated clusters must be in place at those redshifts. Second, strong lensing is a highly non-linear effect. This is mainly because the number of strong lensing events depends sensitively on the number of cusps in, and the length of, the caustic curves of the lenses. Cusps require asymmetric lenses. Asymmetric, substructured clusters are thus much more efficient in producing large arcs than symmetric clusters, provided the individual cluster sublumps are compact enough (Bartelmann, Steinmetz,

Send offprint requests to: Matthias Bartelmann

& Weiss 1995). Both arguments show that the influence of cosmology on the structure and the formation timescale of clusters should strongly affect their ability to form large arcs. Clusters that are being assembled from compact subclusters at redshifts where lenses are most efficient, $0.2 \lesssim z \lesssim 0.4$, should produce many more arcs than clusters which form at later redshifts from sublumps which are less compact.

Does this line of reasoning imply that different cosmological models can be distinguished by the number of arcs that are expected in them? More precisely, does the higher compactness of clusters in low-density universes, and the later formation time of clusters in high-density universes, lead to such different numbers of large arcs that limits on cosmological parameters could be obtained from counting arcs? This is the question addressed by this paper.

In order to pursue it, we use galaxy clusters simulated in a variety of cosmological models. The simulations are described in Sect. 2. The simulated clusters are then investigated as to their strong-lensing effects, following the prescription in Sect. 3. Results are presented in Sect. 4, and summarised in Sect. 5. The paper concludes with a discussion in Sect. 6.

Wu & Mao (1996) already considered the influence of Λ on arc statistics, however with spherically symmetric, non-evolving clusters. They found that this cluster model predicts ~ 2 times more arcs in a low-density, spatially flat universe ($\Omega_0 = 0.3, \Omega_\Lambda = 0.7$) than in an Einstein-de Sitter universe, and that the latter model falls short by a factor of ~ 4 to explain the observed arc abundance. Using a similar model, Hamana & Futamase (1997) pointed out that the expected number of observed arcs increases when the evolution of the background sources is taken into account. Hattori, Watanabe, & Yamashita (1997) included observational selection effects in a study of arc statistics using spherically symmetric cluster models. Using CDM cluster models at a single redshift in an Einstein-de Sitter universe, van Kampen (1996) studied the influence of the normalisation of the power spectrum on the number of arcs per cluster and concluded that the normalisation should be somewhat higher than derived from cluster abundance.

2. Cluster simulations

We use two different sets of cluster simulations. A first set of five clusters is taken from high-resolution cosmological simulations kindly made available by the GIF collaboration, and a second set of four clusters was simulated for the purpose of studying cluster mass profiles in different cosmologies. Different numerical techniques were used for the two simulation sets. They have in common that within each set, the same random phases are used for the initial density field in all cosmological models studied, so that the clusters can be compared individually. The normalisation of the power spectra agrees approximately with the normalisation to the local cluster number density. Apart from improved statistics, the approach using two differently simulated cluster sets allows us to test whether different numerical techniques yield different results for arc statistics. Although the normalisations for the two simulation sets are slightly different, the arc statistics obtained from the two sets individually agree well with each other. The clusters show density profiles $\rho(r)$ that are well fitted by the two-parameter function suggested by Navarro, Frenk, & White (1996). At $z = 0$, we find typical concentration parameters of

$$c \approx \begin{cases} 5 & \text{for S/}\tau\text{CDM} \\ 7 & \text{for } \Lambda\text{CDM} \\ 9 & \text{for OCDM} \end{cases} . \qquad (1)$$

The different values for c reflect the different cluster formation times. When clusters form earlier, their concentration is higher.

2.1. First cluster sample: GIF simulations

2.1.1. The GIF project

The GIF project is a joint effort of astrophysicists from Germany and Israel. Its primary goal is to study the formation and evolution of galaxies in a cosmological context using semi-analytical galaxy formation models embedded in large high-resolution N-body simulations. This is done by constructing merger trees of particle haloes from dark-matter only simulations and placing galaxies into them using a phenomenological modelling (for a detailed description of this procedure as well as results cf. Kauffmann et al. 1997). In order to achieve both good statistics and an accurate treatment of early epochs, high resolution simulations are needed which nevertheless contain a fair sample of the Universe, thus accounting correctly for the influence of large-scale structure on galaxy formation. Those characteristics also make these simulations suitable for the present project.

2.1.2. The simulations

The code used for the GIF simulations is called Hydra. It is a parallel adaptive particle-particle particle-mesh (AP^3M) code (for details on the code cf. Couchman, Thomas, & Pearce 1995; Pearce & Couchman 1997). The current version was developed as part of the VIRGO supercomputing project and was kindly made available by them for the GIF project. The simulations were started on the CRAY T3D at the Computer Centre of the Max-Planck Society in Garching (RZG) on 128 processors. Once the clustering strength required an even larger amount of total memory, they were transferred to the T3D at the Edinburgh Parallel Computer Centre (EPCC) and finished on 256 processors.

A set of four simulations with $N = 256^3$ and with different cosmological parameters was run. Apart from the fiducial Cold Dark Matter (CDM) scenario, denoted SCDM, which has $\Omega_0 = 1$ and $h = 0.5$[1], another $\Omega_0 = 1$ and $h = 0.5$ model was run (τCDM) which has the same shape parameter for the power spectrum, $\Gamma = 0.21$, as the remaining two models. Those are both models with $\Omega_0 = 0.3$, the first one being a flat model with a cosmological constant (ΛCDM, $\Omega_\Lambda = 0.7$, $h = 0.7$), and the last model being an open model (OCDM, $\Omega_\Lambda = 0$, $h = 0.7$). The case

[1] As usual, the Hubble constant is written as $H_0 = 100\,h$ km s^{-1} Mpc^{-1}.

Table 1. Cosmological parameters of the GIF models. Ω_0 and Ω_Λ are the density parameters for matter and the cosmological constant, h is the Hubble parameter, σ_8 is the variance of the density field in spheres of $8\,h^{-1}$ Mpc, and Γ is the shape parameter of the power spectrum. Also given are the size of the cosmological simulation box and the mass $M_{\rm max}$ within $1.5\,h^{-1}$ Mpc radius of the most massive cluster in $10^{15}\,M_\odot$.

Model	Ω_0	Ω_Λ	h	σ_8	Γ	Box Size [Mpc/h]	$M_{\rm max}$
SCDM1	1.0	0.0	0.5	0.60	0.50	85	0.74
τCDM1	1.0	0.0	0.5	0.60	0.21	85	0.74
ΛCDM1	0.3	0.7	0.7	0.90	0.21	141	0.84
OCDM1	0.3	0.0	0.7	0.85	0.21	141	0.85

of the τCDM model is particularly interesting because it shares the $\Omega_0 = 1$ dynamics with the SCDM model, but has a power spectrum with the same shape parameter as the two low-Ω_0 models. A value of $\Gamma = 0.21$ is usually preferred by analyses of galaxy clustering, cf. Peacock & Dodds (1994). This is achieved in the τCDM model despite $\Omega_0 = 1$ and $h = 0.5$ by assuming that a massive neutrino (usually taken to be the τ neutrino) had existed during the very early evolution of the Universe. It must have decayed later, thus shifting the epoch when matter started to dominate over radiation in the Universe, and the neutrino mass and lifetime are chosen such that $\Gamma = 0.21$. For a detailed description of such a model see White, Gelmini, & Silk (1995).

For the low-Ω_0 models, $h = 0.7$ was chosen to achieve $\Gamma = 0.21$. The high-Ω_0 models require $h \sim 0.5$ in order not to conflict with globular-cluster ages and measurements of h.

The GIF simulations adopt the CDM power spectrum, $P(k)$, given by Bond & Efstathiou (1984). In order to completely fix $P(k)$, the normalisation, A, has to be chosen. This can be done on the basis of measurements of the microwave background anisotropies by the COBE satellite. However, this approach suffers from the fact that COBE measured fluctuations on scales much larger than those pertinent to the simulations. Hence, one has to assume that there is no additional physics that could alter the result like, e.g., gravitational waves or a slight tilt of the initial spectrum away from the scale-invariant form. The approach taken here avoids this problem. The mass function of objects in the Universe is very steep at the high-mass end. In other words, massive objects (like clusters of galaxies) are not only rare, but their *abundance* sensitively depends on the amplitude of the power spectrum. White, Efstathiou, & Frenk (1993) introduced this way of fixing the amplitude by determining σ_8, the square root of the variance of the density field smoothed over $8\,h^{-1}$ Mpc spheres, such that the observed abundance of rich clusters is matched. They used the cluster mass function. Recent studies of the cluster X-ray temperature function (Eke, Cole, & Frenk 1996; Viana & Liddle 1996) find similar results. For the low-density GIF simulations, the result by Eke et al. (1996) was taken. For the $\Omega_0 = 1$ simulations, slightly larger values than suggested by Eke et al. (1996) were adopted, according to the earlier result by White et al. (1993). Table 1 summarises the model parameters.

The parameters shown in Table 1 were chosen not only to fulfil cosmological constraints, but also to allow a detailed study of the clustering properties at very early redshifts. The masses of individual particles are $1.0 \times 10^{10}\,h^{-1}\,M_\odot$ and $1.4 \times 10^{10}\,h^{-1}\,M_\odot$ for the high- and low-Ω_0 models, respectively. The gravitational softening was taken to be $30\,h^{-1}$ kpc.

Clusters are obtained from the simulation as follows. High-density regions are searched using a standard friends-of-friends group finder with a linking length of $b = 0.05$ times the mean interparticle separation. This selects only the dense cores of any collapsed object. Around the centres of these, all particles are collected which lie within a sphere of radius $r_{\rm A} = 1.5\,h^{-1}$ Mpc, which corresponds to Abell's radius. These objects are taken as clusters. For our analysis, the five most massive clusters are cut out of the simulation volumes. This procedure needs to be expanded if the centres of two large clusters are closer together than $r_{\rm A}$. In this case usually the more massive cluster is taken, and the other one is deleted from the list. In our case, however, this problem did not occur. The initial density fields for the different cosmologies share the same random phases.

2.2. Second cluster sample

The second cluster sample is simulated using a special multi-mass technique which is explained in detail in Huss, Jain, & Steinmetz (1997). In contrast to the GIF simulations, this technique gives only one massive cluster per run. However, it allows one to study the evolution of one individual cluster without the need for extensive computer resources.

The essential part of the multi-mass technique is the initial particle arrangement. It consists of three spherical layers embedded into a cubic volume, each filled with particles of different mass. The central sphere encompasses the least massive particles and is surrounded by two shells of more massive particles. The rest of the cubic simulation volume is filled up with the most massive particles. The inner sphere must initially be large enough to enclose all particles which end up in a cluster. The gravitational forces on the particles are calculated using a combined GRAPE/PM N-body code assuming periodic boundary conditions. The PM part performs force calculations with periodic boundary conditions for all particles. In the inner three shells, the force is additionally calculated with a PM code using vacuum boundary conditions. This force is subtracted from the periodically computed PM force to obtain the periodic contribution to the force only. This is added to the highly resolved force provided by the GRAPE board for the particles in the inner shells.

The second cluster sample consists of 12 clusters in total. Four clusters are simulated for each of three different cosmologies, which resemble the SCDM, ΛCDM, and OCDM models of the GIF project. The model parameter are summarised in Table 2. All clusters belonging to one cosmological model are part of the same realisation of the corresponding density field. In addition, the phases of the initial Gaussian random field are identical in the three cosmological models.

Table 2. Cosmological parameters of the models for the second cluster sample. The meaning of the symbols is the same as in Tab. 1.

Model	Ω_0	Ω_Λ	h	σ_8	Γ	Box size [Mpc$/h$]	$M_{\max}$
SCDM2	1.0	0.0	0.5	0.60	0.50	144	0.75
ΛCDM2	0.3	0.7	0.7	1.12	0.21	201.6	1.67
OCDM2	0.3	0.0	0.7	1.12	0.21	201.6	1.41

The initial conditions are calculated to match the power spectrum of the different cosmologies. The normalisation of $P(k)$ is chosen as determined by White et al. (1993) for SCDM2, and for OCDM2 and ΛCDM2 it matches the COBE CMB anisotropy measurements. The COBE normalisation yields a slightly higher σ_8 than that derived by Eke et al. (1996). The box size L of the simulation volume is fixed to 288 Mpc in physical coordinates for each run to achieve the same physical spatial resolution in all models. The mass resolution in the central sphere is $4.9 \times 10^{10}\,h^{-1}\ M_\odot$ for the high-density model, and $2.9 \times 10^{10}\,h^{-1}\ M_\odot$ for the low-density models.

Since the simulations result in one massive cluster in the high-resolution region, it can easily be identified by looking for the deepest potential well in this region. However, particular attention has to be paid in order to set up initial conditions with a suitable overdense region in the central sphere, representing the seed for the massive cluster. This is done in the following way. First, a pre-simulation is performed by filling the whole simulation box with particles of the same mass as those in the second layer. At $z = 0$, the cluster-like objects are identified using a special group-finding algorithm (Huss et al. 1997). The particles finally forming these objects define the corresponding overdense region at the initial redshift. The final starting configuration is then centred on one of these regions. By adding small scale power to such a density peak, the clustering properties of the region can be changed. Hence, it is possible that the simulation finally arrives at several low-mass objects rather than at one massive halo. This can be avoided by testing the clustering properties using the Zel'dovich approximation. When propagated to low redshifts with this technique, the particles in the central sphere must form a distinct matter accumulation in the centre rather than showing only filamentary structure.

With this procedure, four suitable overdense regions are identified in the SCDM2 model. For the ΛCDM2 and for the OCDM2 clusters, the starting configurations are centred on the same regions as for the SCDM2 clusters. This is possible since the clustering properties are defined mainly by the local realisation of the random field, which is the same for all three models. However, the final cluster haloes need not represent the most massive clusters in the simulation box.

3. Simulations of arcs

Our method to investigate the arc-formation statistics of the numerical cluster models was described in detail by Bartelmann & Weiss (1994). We will therefore keep the present description brief and refer the reader to that paper for further information. For general information on gravitational lensing, see Schneider, Ehlers, & Falco (1992) or Narayan & Bartelmann (1997), and references therein.

The numerical cluster models yield the spatial coordinates and velocities of discrete particles with equal mass. In order to use them for gravitational lensing, we need to compute the surface mass density distribution of each cluster model in each of the three independent directions of projection. The mass density is first determined by sorting the particles into a three-dimensional grid and subsequently smoothing with a Gaussian filter function. The grid resolution and the width of the Gaussian are adapted to the numerical resolution of the N-body codes in order not to lose spatial resolution by the smoothing of the density field. The smoothed density field is then projected onto the three sides of the computation volume to obtain three surface-density fields for each cluster.

The physical surface mass density fields are then scaled by the critical surface mass density for lensing, which apart from the cosmological parameters depends on the cluster- and source redshifts. We keep the redshift for all sources fixed at $z_\mathrm{s} = 1$, and the clusters are at $0 < z_\mathrm{c} < 1$. This finally yields three two-dimensional convergence fields $\kappa(\boldsymbol{x}, z_\mathrm{c})$ for each cluster model at redshift z_c. From $\kappa(\boldsymbol{x}, z_\mathrm{c})$, all quantities determining the local lens mapping, i.e., the deflection angle and its spatial derivatives, can be computed. We determine the lens properties of the clusters on grids with an angular resolution of $0\farcs3$ in the lens plane in order to ensure that lensed images be properly resolved.

Assuming a single source redshift rather than a source redshift distribution may appear as a fairly crude choice. It is, however, sufficient for our present purpose, for three reasons. (i) $z_\mathrm{s} = 1$ is very close to the average redshift of observed arcs (cf. Kneib & Soucail 1996); (ii) the most likely arc sources with $R \lesssim 23.5$ have measured redshifts of $\sim 0.8 - 1$ (e.g. Lilly et al. 1995); and (iii) varying the source redshift about $z_\mathrm{s} = 1$ while keeping the lens redshift fixed at $z_\mathrm{c} \sim 0.3$ has only a very moderate effect on the critical surface mass density for lensing. Relative to $z_\mathrm{s} = 1$, the latter changes by $\lesssim 10\%$ for $0.8 \le z_\mathrm{s} \le 1.3$, and by $\lesssim 20\%$ for $0.7 \le z_\mathrm{s} \le 2$. Given the other uncertainties of our results, this is a negligible effect.

Sources are then distributed on a regular grid in the source plane. The resolution of this source grid can be kept low close to the field boundaries because there no large arcs occur. Close to the caustics of the clusters, where the large arcs are formed, the source-grid resolution is increased with the increasing strength of the lens. For our later purpose of statistics, sources are weighted with the inverse resolution of the grid on which they are placed. The sources are taken to be intrinsically randomly oriented ellipses with their axis ratios drawn randomly from the interval $[0.5, 1]$, and their axes determined such that their area equals that of circles with radius $0\farcs5$. Although this choice of source properties appears fairly simple, it should not affect the arc statistics because these mainly reflect the local properties of the lens mapping, which are independent of the particular

choice of source size or ellipticity distribution. We checked that a change in average source size did not change the results.

The sources are then viewed through the cluster lenses. All images are classified in the way detailed by Bartelmann & Weiss (1994). Among other things, the classification yields for each image its length L, its width W, and its curvature radius R. In total, we classify the images of about 1.3×10^6 sources.

Knowing the area covered by the cluster fields, and having determined the frequency of occurrence of image properties such as a given length, width, and curvature radius, we can compute cross sections σ for the formation of images with such properties. The arc cross section of a cluster is defined as the area in the *source plane* within which a source has to lie in order to be imaged as an arc. We mostly focus on cross sections for the length-to-width ratio r of arcs. Apart from the image properties, the cross sections depend on redshift, $\sigma = \sigma(z)$.

Given cross sections $\sigma(z)$, we compute the optical depth τ for the formation of large arcs. The optical depth is the fraction of the entire source plane which is covered by cluster cross sections,

$$\tau = \frac{n_\mathrm{c}}{4\pi D_\mathrm{s}^2} \int_0^{z_\mathrm{s}} \mathrm{d}z\,(1+z)^3 \left|\frac{\mathrm{d}V(z)}{\mathrm{d}z}\right| \sigma(z)\;, \qquad (2)$$

where n_c is the present cluster number density, D_s is the angular-diameter distance to the source plane, and $\mathrm{d}V(z)$ is the proper volume of a spherical shell of width $\mathrm{d}z$ about z. The factor $(1+z)^3$ accounts for the cosmological expansion factor.

4. Results

4.1. Cross sections

According to the prescription in Sect. 3, we first calculate cross sections for each individual model cluster, projected in each of the three independent spatial directions. Interpolating in redshift between the redshifts of the model clusters, this yields cross sections $\sigma(z)$ as a function of redshift. We then average these cross sections (i) over the three projection directions and (ii) over all model clusters within a given cosmological model. We thus obtain cross sections for the four cosmological models. Figure 1 shows an example, the cross sections for arcs with length-to-width ratio $r \geq 7.5$.

The averaged cross sections in Fig. 1 reveal huge differences between the cosmological models. While the cross sections for standard CDM (SCDM) and τCDM are comparable, the maximum cross sections for ΛCDM and open CDM (OCDM) exceed that for SCDM by about half and one order of magnitude, respectively, and the redshift range where $\sigma(z) > 0$ is wider in O/ΛCDM than in S/τCDM. Cross sections for other, large values of the length-to-width ratio r, or for large arc lengths, show a qualitatively similar behaviour.

Since the clusters in different cosmologies arise from initial density perturbations with the same random phases, they can also be compared individually rather than statistically. On the whole, the individual clusters show the same qualitative behaviour as the averaged cross sections shown in Fig. 1. Results obtained for each cluster set individually agree well with each other.

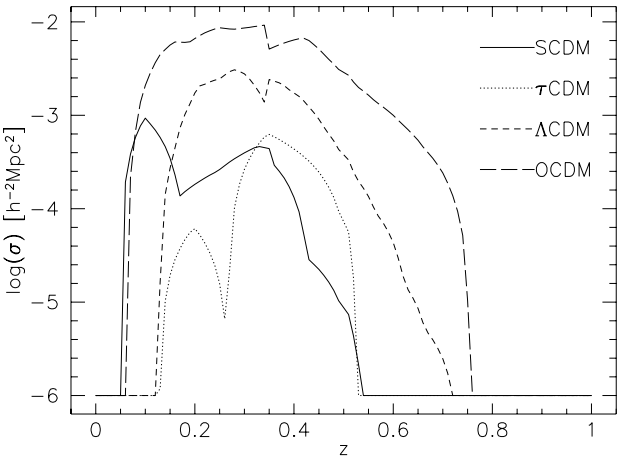

Fig. 1. Averaged cross sections for arc length-to-width ratio $r \geq 7.5$ for clusters in the four different cosmological models, distinguished by line types as indicated. The figure shows that clusters in the τCDM model produce the fewest arcs, and clusters in the open CDM model the most. Note the logarithmic scale of the ordinate: The maxima of the cross sections differ by more than an order of magnitude. The redshift ranges where $\sigma(z) > 0$ are larger in O/ΛCDM than in S/τCDM.

4.2. Arc-cluster redshift

At what redshifts do we expect to find the most clusters that produce large arcs? In other words, clusters at which redshift contribute most to the arc optical depth? To answer this question, we compute the optical depth τ from eq. (2) and the differential optical depth $\mathrm{d}\tau/\mathrm{d}z$, and plot in Fig. 2 the normalised differential optical depth $\tau^{-1}\,\mathrm{d}\tau/\mathrm{d}z$ as a function of redshift for the four cosmological models.

The curves in Fig. 2 show that the differential optical depth peaks around $z \sim 0.3 - 0.4$. The bars inserted in the figure indicate the 1-σ redshift range, $\Delta z \sim 0.1$, and the dots show the average arc-cluster redshift. Although there is a slight tendency that the mean arc-cluster redshift is smallest in the SCDM model, larger for ΛCDM, and largest for τCDM and OCDM, the redshift variances are large enough for the redshift ranges in the cosmological models to overlap. The figure furthermore suggests that the differences between cosmological models are dominated by noise.

4.3. Optical depth

We now compare the optical depth τ for formation of arcs with given length-to-width ratio r in the four cosmological models. As before, the optical depth is calculated from eq. (2). We do not specify the cluster number density n_c yet, but calculate the optical depth per unit cluster density, $n_\mathrm{c}^{-1}\tau$. Results are shown in Fig. 3.

Figure 3 confirms the trends indicated by the cross sections in Fig. 1, but allows to compare optical depths for a wide range

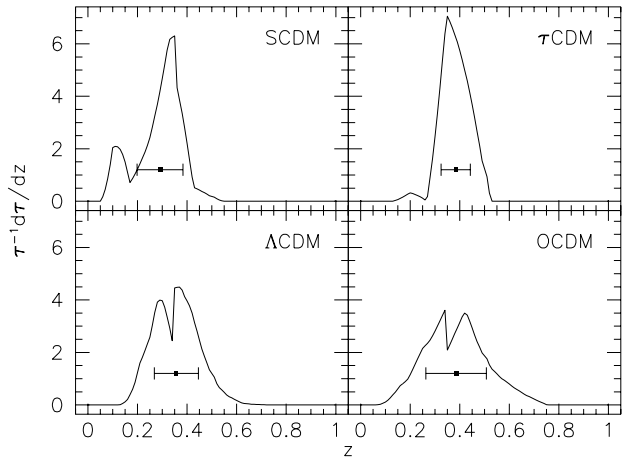

Fig. 2. Normalised, differential optical depth as a function of redshift, for arcs with length-to-width ratio $r \geq 7.5$. The curves indicate the most probable redshift for a cluster forming arcs for the four cosmological models used. The bars show the 1-σ redshift range, the dots indicate the mean arc-cluster redshift. The plot shows that there is no significant difference in arc cluster redshift between the four cosmological models.

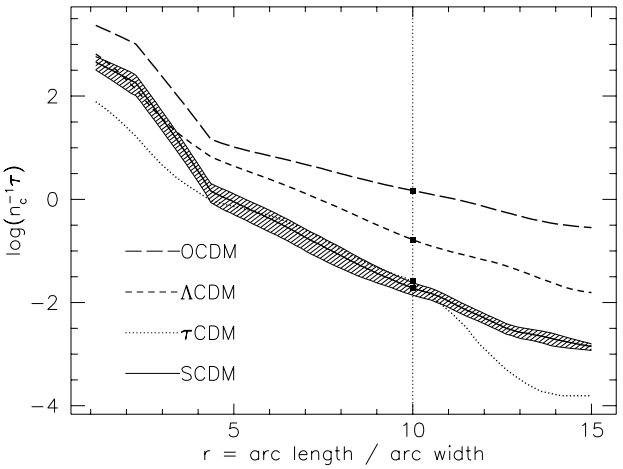

Fig. 3. Optical depth for arc formation as a function of arc length-to-width ratio r, for the four different cosmological models. The optical depth for the τCDM and the standard CDM models are comparable for intermediate length-to-width ratios r. For large r, the optical depth is smallest for the τCDM model. The largest optical depth is produced by clusters in the open CDM model, followed by those in the ΛCDM model. For $r \sim 10$, the optical depths for open CDM, ΛCDM, and standard CDM differ by about an order of magnitude each. The hatched area around the SCDM curve indicates 1-σ bootstrap errors.

of arc length-to-width ratios r. There is an interval at intermediate r, $5 \lesssim r \lesssim 10$, where the optical depths for SCDM and τCDM are almost equal. Only at $r \gtrsim 10$ does the optical depth in τCDM models drop below that of SCDM models. For $r \gtrsim 4$, the optical depth for ΛCDM models is constantly higher than that for SCDM models by a factor of ~ 10. The optical depth for the OCDM model is highest, exceeding the SCDM value by up to ~ 2 orders of magnitude at large r.

The hatched region around the SCDM curve illustrates 1-σ errors, which we obtained by bootstrapping the cluster sample. They give an impression of the uncertainty of the optical depth due to the limited number of clusters in our samples. The uncertainty due to the specific realisation of the lensed background galaxy sample are smaller by about a factor of five.

5. Discussion

5.1. Results

Our main result is that the optical depths for large arcs, with length-to-width ratio $r \geq 10$, differ by orders of magnitude for the different cosmologies. Generally, clusters in the SCDM and τCDM models produce the smallest optical depth. For $r \sim 10$, the optical depths for these two models are comparable, but for larger r, the optical depth in the τCDM model falls below that in the SCDM model. In the ΛCDM model, the arc optical depth is larger by about an order of magnitude than for SCDM, and the optical depth is largest in the OCDM model, exceeding the SCDM optical depth by about two orders of magnitude. We emphasise that these results are independent of whether our cluster samples are in any sense *complete* or not, because the simulations are designed such that the clusters can be compared individually. Our conclusions do, however, rest on the assumption that the simulated clusters are *typical* for the clusters with the largest mass in each of the cosmological models. We believe that this is guaranteed by the large size of the cosmological simulation volumes from which the clusters were taken.

It is a combination of effects that leads to the large difference in arc optical depth across the cosmological models that we have investigated. (i) Clusters form earlier in low-density than in high-density universes. In SCDM, normalised to the cluster abundance, the formation of such clusters which would in principle be massive enough for strong lensing is delayed to such low redshifts that they fail to be efficient lenses for sources at redshifts $z_s \sim 1$. (ii) For low-density universes, the proper volume per unit redshift is larger than for high-density universes. Given the observed number density of clusters today, this volume effect increases the number of clusters between the source sphere and the observer when Ω_0 is small. (iii) Clusters that form early are more concentrated than clusters that form late. Clusters in low-density universes therefore reach higher central surface mass densities than clusters in high-density universes. (iv) Strong gravitational lensing is a highly non-linear effect. This is because the arc cross section of a cluster sensitively depends on the length of the caustic curve and the number of cusp points contained in it. The properties of the caustic curve do not only depend on the surface mass density, but also on the tidal field of a cluster, which is influenced by the cluster morphology. (v) Because of (iv), asymmetric clusters are much more efficient in producing large arcs than symmetric clusters (Bartelmann et al. 1995). The degree of substructure of a cluster is therefore very important for arc statistics. While clusters are in the process of formation, they are expected to be highly asym-

metric. If this happens at redshifts where lensing is efficient for a given source population, the asymmetric cluster morphology further increases the strong-lensing cross section. Most clusters in OCDM and ΛCDM form at $z \sim 0.3$, exactly where lensing is most efficient for sources at $z_\mathrm{s} \sim 1$. Clusters in SCDM and τCDM form later, at $z \sim 0.1$, where their lensing efficiency and that of their sublumps is already suppressed by the lensing geometry. Although clusters in S/τCDM form later than in O/ΛCDM and should therefore be more asymmetric, the sublumps in O/ΛCDM clusters are more compact and thus tend to persist for a longer time after merging with the cluster.

5.2. Illustration

A simple Press-Schechter type argument illustrates the influence of formation time and cosmic volume. According to Press & Schechter (1974), the (comoving) fraction of the cosmic matter that is contained in clusters is

$$F_\mathrm{c}(z) = \frac{1}{2}\,\mathrm{erfc}\left(\frac{\delta_\mathrm{c}}{\sqrt{2}\,\sigma_R\,\mathscr{D}(z)}\right)\,, \tag{3}$$

with $\delta_\mathrm{c} \approx 1.686$, σ_R the variance of the density contrast on cluster scales today, and $\mathscr{D}(z)$ the (cosmology-dependent) linear growth factor of density perturbations. The cluster fraction at redshift z, normalised to the present cluster fraction, provides an estimate for the change in cluster number density with redshift. Multiplying with the proper cosmic volume $4\pi\,D^2(z)\,|\mathrm{d}(ct)/\mathrm{d}z|\,\mathrm{d}z$ of a shell of width $\mathrm{d}z$ and the squared effective lensing distance $D_\mathrm{eff}(z, z_\mathrm{s})$ yields an estimate for the number of efficient lensing clusters per redshift interval,

$$\frac{\mathrm{d}N_\mathrm{lens}}{\mathrm{d}z} = F_\mathrm{c}(z)\times(1+z)^3\times D^2_\mathrm{eff}(z,z_\mathrm{s})\times 4\pi\,D^2(z)\,\left|\frac{\mathrm{d}(ct)}{\mathrm{d}z}\right|\,, \tag{4}$$

because the cross section per cluster should scale approximately with $D^2_\mathrm{eff}(z, z_\mathrm{s})$. This quantity is plotted in Fig. 4 for $\Omega_0 = 1$ and $\Omega_0 = 0.3$, with $\Omega_\Lambda = 0$. Of course, this simple estimate completely neglects the influence of the change in cluster concentration across the cosmological models, and the non-linearities of the strong lensing effect. However, it suffices to demonstrate that large differences in the arc cross section are expected between high- and low-density universes.

5.3. Influence of "missing clusters"

All cosmological simulation volumes from which we have taken the cluster models are of order a few times $10^6\,h^{-3}\,\mathrm{Mpc}^3$. Since the cluster mass function is very steep, we are therefore likely to miss the most massive clusters. In order to estimate their influence on the arc cross sections, we have repeated the arc simulations for SCDM with surface-mass densities rescaled to higher cluster mass. Let M_0 and $M > M_0$ be the original and rescaled cluster masses, respectively. Then, we take

$$\kappa'(\boldsymbol{x}, z_\mathrm{c}, M) = \left(\frac{M}{M_0}\right)^{1/3}\,\kappa\left[\left(\frac{M_0}{M}\right)^{1/3}\boldsymbol{x}, z_\mathrm{c}, M_0\right] \tag{5}$$

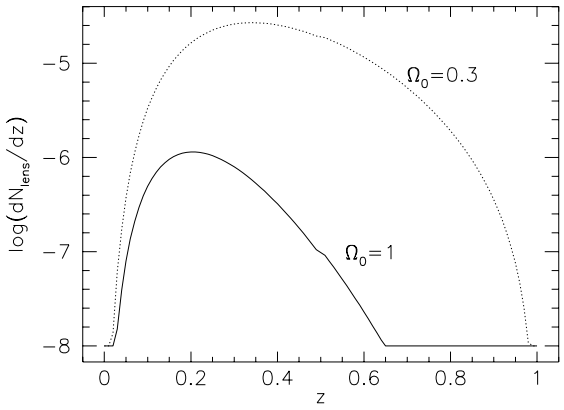

Fig. 4. Estimate for the number of efficient lensing clusters per redshift interval, $\mathrm{d}N_\mathrm{lens}/\mathrm{d}z$, as given in eq. (4). Results for $\Omega_0 = 1$ and $\Omega_0 = 0.3$, both with $\Omega_\Lambda = 0$, are plotted, as indicated. The figure illustrates that the delayed formation of clusters in a high-density universe, combined with the effects of lensing efficiency and cosmic volume, already account for a large difference in the expected number of arcs.

for the rescaled surface-mass density and compute the arc cross section from that. In effect, we calculate the arc cross section $\sigma(z_\mathrm{c}, M)$ of a cluster of similar structure as the original one, but with higher total mass. For each cluster model at redshift z_c, we then average the arc cross sections over mass, weighted by the Press-Schechter cluster mass function $n(M)$,

$$\langle\sigma(z_\mathrm{c})\rangle = \frac{\int \mathrm{d}M\,n(M)\,\sigma(z_\mathrm{c}, M)}{\int \mathrm{d}M\,n(M)}\,. \tag{6}$$

Finally, we compute mass-averaged optical depths $\langle\tau\rangle$ by substituting $\langle\sigma(z_\mathrm{c})\rangle$ for $\sigma(z_\mathrm{c})$ in eq. (2).

We found that $\langle\tau\rangle$ differs from τ only by 10-15 per cent. Although the arc cross section is a fairly steep function of mass, the increase in σ is more than compensated by the steep decrease of the cluster mass function. For example, quadrupling the masses of the τCDM clusters increases the averaged cross section for arcs with $r \geq 10$ by about two orders of magnitude, but decreases the cluster mass function by about three orders of magnitude, almost completely cancelling the effect of the larger arc cross section. For clusters in the other cosmological models, the change in the optical depth should be smaller than that in τCDM. Clusters with higher masses than those contained in our sample can therefore safely be neglected.

We have only studied the most massive clusters found in each cosmological simulation. Even then, the least massive clusters in each sample contribute little or nothing to the arc optical depth. Extending our samples by including less massive clusters would therefore change the arc optical depth negligibly or not at all.

Since we select the most massive clusters at redshift zero and study their progenitors, it could be that at higher redshift other clusters in the cosmological simulations would be more massive. In other words, it is not immediately clear that the progenitors of the most massive clusters are also the most massive clusters

present at higher redshift. In order to test that, we selected the τCDM model, where clusters form at the lowest redshifts, and checked whether the progenitors of the our sample of the five most massive clusters is identical with the sample of the five most massive clusters at the redshifts relevant for lensing. This turned out to be the case. In the other models, where clusters form at higher redshifts, possible misidentifications are even less likely than in τCDM.

Given these results, we are confident that our cluster samples fairly reflect those clusters that dominate the optical depth for the formation of large arcs.

6. Comparison with observations

So can we constrain cosmological parameters through arc statistics? For that, we would have to compare the number of observed arcs to that predicted by our models. This comparison is hampered by the fact that there is no complete sample of observed clusters selected by *mass*, as it should be for a fair comparison. There is one cluster sample, however, whose definition comes close to this criterion, namely the EMSS sample of X-ray bright clusters, for which the X-ray luminosity in the EMSS energy band is $L_\mathrm{X} \geq 2\times10^{44}\,\mathrm{erg\,s^{-1}}$ (h = 0.5, q_0 = 0.5). The number density of such clusters is estimated to be $n_\mathrm{c} \sim 2\times10^{-6}\,h^3\,\mathrm{Mpc}^{-3}$ (Le Fèvre et al. 1994). Arc surveys in this sample have shown that the number of arcs with $r \geq 10$ and a limiting magnitude of B = 22.5 (or R = 21.5; these are the arc criteria set up by Wu & Hammer 1993) is roughly $\sim 0.2-0.3$ per cluster (Le Fèvre et al. 1994; Gioia & Luppino 1994).

Clusters with $L_\mathrm{X} \geq 2\times10^{44}\,\mathrm{erg\,s^{-1}}$ should be fairly represented by the massive simulated clusters in our samples. Having velocity dispersions $\gtrsim 800\,\mathrm{km\,s^{-1}}$, the empirical relation between velocity dispersion and X-ray luminosity obtained by Quintana & Melnick (1982) implies X-ray luminosities in the right range. We can therefore assume that the arc cross sections of our simulated clusters are typical for X-ray luminous clusters in the EMSS survey.

The curves in Fig. 3 give $n_\mathrm{c}^{-1}\,\tau$. Using the number density of bright EMSS clusters given above,

$$\tau(r\geq10)\sim\begin{cases}2.9\times10^{-6} & \text{(OCDM)}\\ 3.3\times10^{-7} & (\Lambda\text{CDM})\\ 4.4\times10^{-8} & (\text{S}/\tau\text{CDM})\end{cases}. \qquad (7)$$

Since the whole sky has $\sim 4.1\times10^4$ square degrees, the total solid angle in which sources at $z_\mathrm{s}\sim1$ are imaged as large arcs with $r \geq 10$ is

$$\delta\omega\sim\begin{cases}1.2\times10^{-1}\,\mathrm{sq.\,deg.} & \text{(OCDM)}\\ 1.4\times10^{-2}\,\mathrm{sq.\,deg.} & (\Lambda\text{CDM})\\ 1.8\times10^{-3}\,\mathrm{sq.\,deg.} & (\text{S}/\tau\text{CDM})\end{cases}. \qquad (8)$$

The sources which are imaged as arcs with the above properties, $r \geq 10$ and $R \leq 21.5$ correspond to sources with $R \lesssim 23.5$ because of the magnification. Taking the number densities compiled and measured by Smail et al. (1995), there are $\sim 2\times10^4$ such sources per square degree. The average redshift of such sources is $\sim 0.8-1$ (e.g. Lilly et al. 1995). Since the average arc-cluster redshift in our models is at $z_\mathrm{c}\sim0.3-0.4$, the exact redshift of sources at $z\sim0.8-1$ has only very little influence; the critical surface mass density changes by $\sim 10\%$ when sources are shifted from z = 0.8 to z = 1.2. It follows that the number of such arcs on the whole sky expected from our simulations is

$$N_\mathrm{arcs}\sim\begin{cases}2400 & \text{(OCDM)}\\ 280 & (\Lambda\text{CDM})\\ 36 & (\text{S}/\tau\text{CDM})\end{cases}. \qquad (9)$$

There are $\sim$ 7500 clusters on the sky which match the criteria of the EMSS bright cluster sample (Le Fèvre et al. 1994). Taking the number of arcs per cluster found in the EMSS clusters, the expected number of arcs on the whole sky is $\sim 1500-2300$. Despite the obvious uncertainties in this estimate, *the only of our cosmological models for which the expected number of arcs comes near the observed number is the open CDM model*. The others fail by one or two orders of magnitude. The large differences in arc optical depth between the cosmological models investigated makes this result fairly insensitive to moderate uncertainties. It therefore appears fair to conclude that arc statistics in the framework of cluster-normalised CDM models demands that Ω_0 is low, and that Ω_Λ is small. Conversely, if $\Omega_0\sim1$, clusters have to form earlier than in our models. We estimate with the simple Press-Schechter approach sketched above that in order to achieve that, $\sigma_8\sim1.2-1.3$ would be necessary in the SCDM case.

We have neglected the potential influence of cD galaxies or cooling flows on the arc cross sections that could increase the central surface mass densities of the clusters and thus also their arc cross sections. Most probably, this influence is small compared to the huge differences between the cosmological models. Nonetheless, we will study this issue in detail in a further paper. Individual cluster galaxies can increase the total arc cross section, most probably by a factor of $\lesssim 2$ (Bézecourt, Pelló, & Soucail 1997). They can also affect arc morphologies, e.g. by making arcs thinner or splitting them into several parts. Again, such effects are small compared to the differences between cosmological models found here, but they must be addressed once more detailed constraints on cosmological parameters are to be placed. Then, observing conditions must also be taken into account.

Acknowledgements. We have benefited from many instructive discussions, particularly with Suvendra Dutta, Gus Evrard, Eelco van Kampen, Shude Mao, Houjun Mo, Julio Navarro, Peter Schneider, and Simon White. Matthias Steinmetz and Achim Weiss contributed a lot to the numerical code which we used to automatically classify the arcs. This work was supported in part by the Sonderforschungsbereich 375 of the Deutsche Forschungsgemeinschaft.

References

Bartelmann, M., Weiss, A., 1994, A&A, 287, 1
Bartelmann, M., Ehlers, J., Schneider, P., 1993, A&A, 280, 351

Bartelmann, M., Steinmetz, M., Weiss, A., 1995, A&A, 297, 1
Bézecourt, J., Pelló, R., Soucail, G., 1997, A&A, submitted; SISSA preprint astro-ph/9707169
Bond, J.R., Efstathiou, G., 1984, ApJ, 285, L45
Buote, D.A., Tsai, J.C., 1995a, ApJ, 439, 29
Buote, D.A., Tsai, J.C., 1995b, ApJ, 452, 522
Couchman, H.M.P., Thomas, P.A., Pearce, F.R., 1995, ApJ, 452, 797
Crone, M.M., Evrard, A.E., Richstone, D.O., 1994, ApJ, 434, 402
Crone, M.M., Evrard, A.E., Richstone, D.O., 1996, ApJ, 467, 489
Crone, M.M., Governato, F., Stadel, J., Quinn, T., 1997, ApJ, 477, L5
Eke, V.R., Cole, S., Frenk, C.S., 1996, MNRAS, 282, 263
Evrard, A.E., Mohr, J.J., Fabricant, D.G., Geller, M.J., 1993, ApJ, 419, L9
Gioia, I.M., Luppino, G.A., 1994, ApJS, 94, 583
Hamana, T., Futamase, T., 1997, MNRAS, 286, L7
Hattori, M., Watanabe, K., Yamashita, K., A&A, 319, 764
Huss, A., Jain, B., Steinmetz, M., 1997, MNRAS, submitted (preprint astro-ph/9703014)
Jing, Y.P., Mo, H.J., Börner, G., Fang, L.Z., 1995, MNRAS, 276, 417
van Kampen, E., 1996, in: Mapping, Measuring and Modelling the Universe, Proc. Valencia 1995. eds. P. Coles, V. Martínez.
Kauffmann, G.A.M., Colberg, J.M., Diaferio, A., White, S.D.M., 1997, in preparation
Kneib, J.-P., Soucail, G., 1996, IAU Symposium 173, 113
Lacey, C., Cole, S., 1993, MNRAS, 262, 627
Lacey, C., Cole, S., 1994, MNRAS, 271, 676
Le Fèvre, O., Hammer, F., Angonin, M.-C., Gioia, I.M., Luppino, G.A., 1994, ApJ, 422, L5
Lilly, S.J., Tresse, L., Hammer, F., Crampton, D., Le Fèvre, O., 1995, ApJ, 455, 108
Navarro, J.F., Frenk, C.S., White, S.D.M., 1996, ApJ, 462, 563
Mohr, J.J., Evrard, A.E., Fabricant, D.G., Geller, M.J., 1995, ApJ, 447, 8
Narayan, R., Bartelmann, M., 1997, in: Formation of Structure in the Universe, Proc. 1995 Jerusalem Winter School. eds. A. Dekel, J.P. Ostriker. Cambridge Univ. Press
Peacock, J.A., Dodds, S.J., 1994, MNRAS, 267, 1020
Pearce, F.R., Couchman, H.M.P., 1997, New Astronomy, 2, 411
Press, W.H., Schechter, P.L., 1974, ApJ, 187, 425
Quintana, H., Melnick, J., 1982, AJ, 87, 972
Richstone, D.O., Loeb, A., Turner, E.L., 1992, ApJ, 393, 477
Schneider, P., Bartelmann, M., 1997, MNRAS, 286, 696
Schneider, P., Ehlers, J., Falco, E.E., 1992, Gravitational Lenses. Heidelberg, Springer Verlag
Smail, I., Hogg, D.W., Yan, L., Cohen, J.G., 1995, ApJ, 449, L105
Viana, P.T.P., Liddle, A.R., 1996, MNRAS, 281, 323
White, M., Gelmini, G., Silk, J., 1995, Phys. Rev. D, 51, 2669
White, S.D.M., Efstathiou, G., Frenk, C.S., 1993, MNRAS, 262, 1023
Wilson, G., Cole, S., Frenk, C.S., 1996, MNRAS, 282, 501
Wu, X.-P., Hammer, F., 1993, MNRAS, 262, 187
Wu, X.-P., Mao, S., 1996, ApJ, 463, 404

This article was processed by the author using Springer-Verlag LaTeX A&A style file *L-AA* version 3.